Asian Journal of Chemistry; Vol. 34, No. 12 (2022), 3132-3144

ASIAN JOURNAL OF CHEMISTRY

https://doi.org/10.14233/ajchem.2022.24012

Dielectric, AC Conductance of Chalcone Moiety, Metal Oxide Nanocomposite Doped Thin Polymer Film: Synthesis and Characterization

B. AYYANAR[1], J. SURESH[1], V. THANGARAJ[1], S. KARTHIKEYAN[2], A. ARUN[1] and M. KAYALVIZHI[1,*]

[1]Department of Chemistry, Kalaignar Karunanidhi Government Arts College, Tiruvannamalai-606603, India
[2]Department of Physics, Madras Christian College, Chennai-600059, India

*Corresponding author: E-mail: kayalpappa78@gmail.com

Received: 8 August 2022; *Accepted*: 9 September 2022; *Published online*: 25 November 2022; AJC-21037

For conducting use, an organic molecule chalcone (1-(2,4-dichlorophenyl)-3-(4-hydroxy-phenyl)-prop-2-en-1-one (DCHP) and metal oxide nanocomposite (MONC) doped polymer thin films were prepared. In addition, polyvinyl alcohol (PVA) and chitosan (CS) was utilized as a host polymer. The features of successfully prepared thin polymer films were characterized. The XRD analysis revealed the nano-sized (40-150 nm), crystalline phases and semi-crystalline behaviour of polymer films. The XPS and EDX confirmed the elements of PVA, CS, DCHP, MONC4 and MONC5, as well as the oxidation states of MONC4 and MONC5 sample films. The morphology of the prepared polymer film revealed an even distribution, a smooth surface and a blossoming flower-like structure from the SEM results. The TGA study revealed the multi-stage decomposition upon heating, but no complete decomposition for the produced film containing MONC4 and MONC5 thin films. The bonding between doped materials and the host polymer in the film was confirmed by FT-IR studies. The produced thin polymer composite film containing metal oxide nanocomposites and DCHP exhibited a high dielectric property and high AC conductance of 1.12×10^{-6} S cm^{-1} at room temperature.

Keywords: Chitosan, Polyvinyl alcohol, Chloro chalcone, Nanocomposite, Polymer film, AC Conductance, Dielectric.

INTRODUCTION

Researchers have been working for a long period of time to discover an efficient electric conducting polymer film (ECPF) because conducting polymer film is so important in batteries and other electrical devices [1-4]. Enhancements such as specific strength, specific modulus, corrosion resistance and thermal stability are frequently added to conducting polymer films [5-7]. Different polymers, including naturally derived polymers like starch, chitin, cellulose and chitosan (CS), are utilized as hosting materials for performing polymer film synthesis [8,9]. Polyvinyl alcohol (PVA), among other polymers, is frequently utilized for the manufacturing of polymeric composite films due to its water solubility, mechanical strength, ease of handling, non-toxic properties and high stability [10]. Polymer nanocomposites outperform traditional micro and macrocomposites in terms of characteristics and may be created by adding nano-sized particles into polymer matrices. Polymer nanocomposites are being intensively studied for a wide range of applications since, they combine the multifunctional characteristics of the organic and inorganic materials. These kinds of composites, which are made from a transparent polymer host matrix containing metal oxide nanoparticles, have attracted the attention of research groups due to their potential technological applications, such as transistors for electronic switches, energy storage electrodes, solar cells and bio-ink for 3D bio-printing [11,12].

Zinc oxide is a n-type semiconductor with a large band gap (3.3 eV). When compared to bulk ZnO, nanocrystalline ZnO possesses superior optical, mechanical, electrical and chemical characteristics. Nano-sized ZnO has prospective applications in the fields of effect transistors, nano-generators, solar cells and photocatalysis [13]. Thermally stable chitosan-based PVA-ZnO bio-nanocomposites were produced and evaluated for organic decolorization [14]. In general, following nanocomposite synthesis with metal or metal oxide nanoparticles, the mechanical and thermal characteristics of PVA were enhanced. When PVA dissolves in aqueous media, it loses its mechanical and thermal characteristics due to the breakdown of inter and intramolecular hydrogen bonding. However, when the nanocomposite is formed, nanofillers fill the gaps between the

polymer strands. Thus, the interaction is influenced by a variety of variables, such as the polarity of the PVA and the functional groups accessible to the nanofillers. Cerium nanoparticles are gaining popularity due to their beneficial features, such as high surface area, large pore volume, strong thermal stability, ionic conductivity and dielectric properties and applied as electrolyte materials for solid oxide fuel cells [15], catalysts [16], gas sensors [17], hydrogen storage materials [18,19], superconducting microwave devices [20], photovoltaic applications [21], *etc*.

The literature on polymer composites of complex metal oxide nanocomposites is very limited, but several articles are available on nanometal oxide doped polymeric composite films, so we intend to prepare a polymer composite film containing a complex metal oxide nanocomposite and find its electrical properties. There was a scarcity of literature on versatile organic molecules like chalcone added to polymeric composite films. For optical use, organic compounds have been added to PVA-like polymers [22,23]. Study on the organic and inorganic compounds added to polymeric composite films has also decreased, so it is decided to prepare a polymer composite film having both organic and inorganic materials. This article reports the preparation, characterization and electrical properties of metal oxide nanocomposite doped thin polymer film containing polyvinyl alcohol (PVA) and chitosan (CS).

EXPERIMENTAL

Aldrich Chemicals provided PVA (m.w. 79,000-90,000) and chitosan (CS) at high density and used as received. Glacial acetic acid was supplied by S.D. Fine Chemicals and 5.6% diluted glacial acetic acid (GAA) was used as solvent. As doping agents, metal oxide nanocomposite MONC4 ($Ce_{3.55}$, $Sr_{1.45}$, $Fe_{4.55}$, $Zn_{0.45}$, $O_{14+\delta}$), MONC5 ($Ce_{3.55}$, $Cs_{2.90}$, $Fe_{4.55}$, $Zn_{0.45}$, $O_{14+\delta}$) [24] and 1-(2,4-dichlorophenyl)-3-(4-hydroxy-phenyl)-prop-2-en-1-one (chalcone, DCHP) were synthesized by reported methods [25].

Characterization: An FT-IR ALPHA Bruker instrument was used to characterize the produced thin polymer composite film. A DuPont 951 analyzer was used to determine the thermal behaviour of the produced thin film. In an inert environment with a nitrogen gas flow rate of 100 mL/min, the film was heated from 30 to 800 ºC at a heating flow rate of 10 ºC/min. The XRD diffraction pattern was discovered using a Siemens D5005 diffractometer (Cu*K*α (= 0.154178 nm)) radiation. The elemental characteristics of the produced film were determined using the XPS (ESCA-3 mark II (Al K-1486.6 eV)) instrument. The elemental characteristics of the produced polymer films are studied using EDX (TESCAN MIRA 3 XMU) instrument. Surface morphology was examined using a FE-SEM model ULTRA-55 and conductivity was determined using a HOIOKI-3532 LCZ meter.

Synthesis of polymer composite conducting thin films: Using a well-known method, a solid thin conducting polymer composite film was prepared. The different weight percentages of PVA, CS and DCHP (Table-1) were placed in an round bottom flask containing 5.6% of 50 mL of GAA. Stirred the solution for 3 h at 50 ºC, then pour it into a perti dish. The evaporation of the GAA solvent produces a thin layer with a size of 0.03 cm^{-1}. The dried thin polymer composite layer was peeled off and analyzed.

Synthesis of a C1 polymer film: PVA (1.000 g) and CS (0.990 g) were placed in an round bottom flask containing 50 mL of 5.6% GAA, swirled to achieve a uniform solution and then 0.010 g of MONC4 was added and stirred for 3 h at 50 ºC before being placed in a petridish. The evaporation of GAA leads to the formation of a thin polymer composite film. FT-IR (cm^{-1}): 3562 (OH, CS), 3381 (OH of DCHP), 3177 (OH of PVA), 3022 (arom. CH of DCHP), 2925 (alkane), 2853 (C-H), 1600 (CO of DCHP), 1592 (CH=CH of DCHP), 1606, 1535 (C-O of CS), 1413 (C-O-C of CS), 611 (out of plane NH of CS).

Synthesis of C1AC1 polymer film: PVA (1.000 g) and CS (0.980 g) were placed in an round bottom flask containing 50 mL of 5.6% GAA, swirled to obtain a uniform solution and then 0.010 g of MONC4 and 0.010 g of DCHP were added and stirred for 3 h at 50 ºC before being placed in a petridish. The evaporation of GAA leads to the formation of a thin polymer composite film. FT-IR (KBr, ν_{max}, cm^{-1}): 3560 (OH, CS), 3380 (OH of DCHP), 3255 (OH of PVA), 3021 (arom. CH of DCHP), 2924 (alkane), 2850 (C-H), 1647 (CO of DCHP), 1552 (CH=CH of DCHP), 1170 (C-O-C of CS), 709 (out of plane NH of CS), 563 (Fe-O), 509 (Zn-O).

Synthesis of D1 polymer film: PVA (1.000 g) and CS (0.990 g) were placed in an round bottom flask containing 50 mL of 5.6% GAA, swirled to achieve a uniform solution and then 0.010 g of MONC5 was added and stirred for 3 h at 50 ºC before being placed in a petridish. The evaporation of GAA solvent leads to the formation of a thin polymer composite film. FT-IR (KBr, ν_{max}, cm^{-1}): 3562 (OH, CS), 3385 (OH of DCHP), 3257 (OH of PVA), 3026 (arom. CH of DCHP), 2929 (alkane), 2853 (C-H), 1647 (CO of DCHP), 1532 (C-O of CS), 1326 (C-O-C of CS), 563 (Fe-O), 509 (Zn-O), 447 (Ce-O).

D1AC1 polymer film synthesis: PVA (1.000 g) and CS (0.980 g) were placed in an round bottom flask containing 50 mL of 5.6% GAA, swirled to obtain a uniform solution and then 0.010 g of MONC5 and 0.010 g of DCHP were added and stirred for 3 h at 50 ºC before being placed in a petri dish.

TABLE-1
WEIGHT PERCENTAGE OF PVA, Cs, METAL OXIDE NANO COMPOSITE ($Ce_{3.55}$, $Sr_{1.45}$, $Fe_{4.55}$, $Zn_{0.45}$, $O_{14+\delta}$) & ($Ce_{3.55}$, $Cs_{2.90}$, $Fe_{4.55}$, $Zn_{0.45}$, $O_{14+\delta}$), DCHP

Polymer film code	Wt.% of PVA (g)	Wt.% of Cs (g)	DCHP (g)	Wt.% metal oxide nano composite ($Ce_{3.55}$, $Sr_{1.45}$, $Fe_{4.55}$, $Zn_{0.45}$, $O_{14+\delta}$) (g)	Wt.% metal oxide nano composite ($Ce_{3.55}$, $Cs_{2.90}$, $Fe_{4.55}$, $Zn_{0.45}$, $O_{14+\delta}$) (g)
C1	1	0.990	–	0.01	–
C1AC1	1	0.980	0.01	0.01	–
D1	1	0.990	–	–	0.01
D1AC1	1	0.980	0.01	–	0.01

The evaporation of glacial acetic acid leads to the formation of a thin polymer composite film. FT-IR (KBr, ν_{max}, cm^{-1}): 3563 (OH, CS), 3386 (OH of DCHP), 3257 (OH of PVA), 3027 (arom. CH of DCHP), 2929 (alkane), 2853 (C-H), 1647 (CO of DCHP), 1559 (CH=CH of DCHP), 1606, 1535 (C-O of CS), 1174 (C-O-C of CS), 713 (out of plane NH of CS).

RESULTS AND DISCUSSION

FT-IR studies: Figs. 1 and 2 show the FT-IR spectra of the prepared films C1, C1AC1, D1 and D1AC1. The stretching frequency measured at around 3257 cm^{-1} confirmed that the hydroxyl functional group of PVA is not engaged in any chemical interaction with the doping agents used, MONC4 or MONC5 or DCHP. This has also been noted before for this type of polymer composite film [26]. Another polymer, CS, containing functional groups –OH and –NH, had no chemical interaction with the doping agents used. The –OH of CS stretching appeared at about 3585 cm^{-1}, whereas –NH of CS appeared at ~611 cm^{-1} (out of plane frequency).

The FT-IR spectrum of the prepared polymer film C1 exhibits a distinctive peak at 563 cm^{-1}, which verified the existence of Fe-O, whereas a peak at 424 cm^{-1} corresponds to the stretching frequency of Sr and a peak at 447 cm^{-1} belongs to Ce, with Zn-O stretching frequency at 509 cm^{-1}. The prepared film C1AC1, which includes MONC4 and DCHP chalcone, displays a typical peak for metal oxide as seen in C1 as well as some stretching frequency that corresponds to the added chalcone. The peaks at 1647 cm^{-1} and 1552 cm^{-1} correspond to the DCHP C=O and C=C frequencies, respectively. These two peaks may also be seen in the thin film D1AC1, which also includes DCHP (Fig. 2). The only difference between C1 and D1 polymer films is that the former includes Sr-O while the latter contains Cs-O. The Sr-O stretching frequency was at 424 cm^{-1} (Fig. 1), while the Cs-O stretching frequency was 1134 cm^{-1} (Fig. 2). The stretching frequency of the functional groups PVA, CS and DCHP were shown as such and it was determined that there was no chemical interaction between the host polymer PVA, CS and the doping agents.

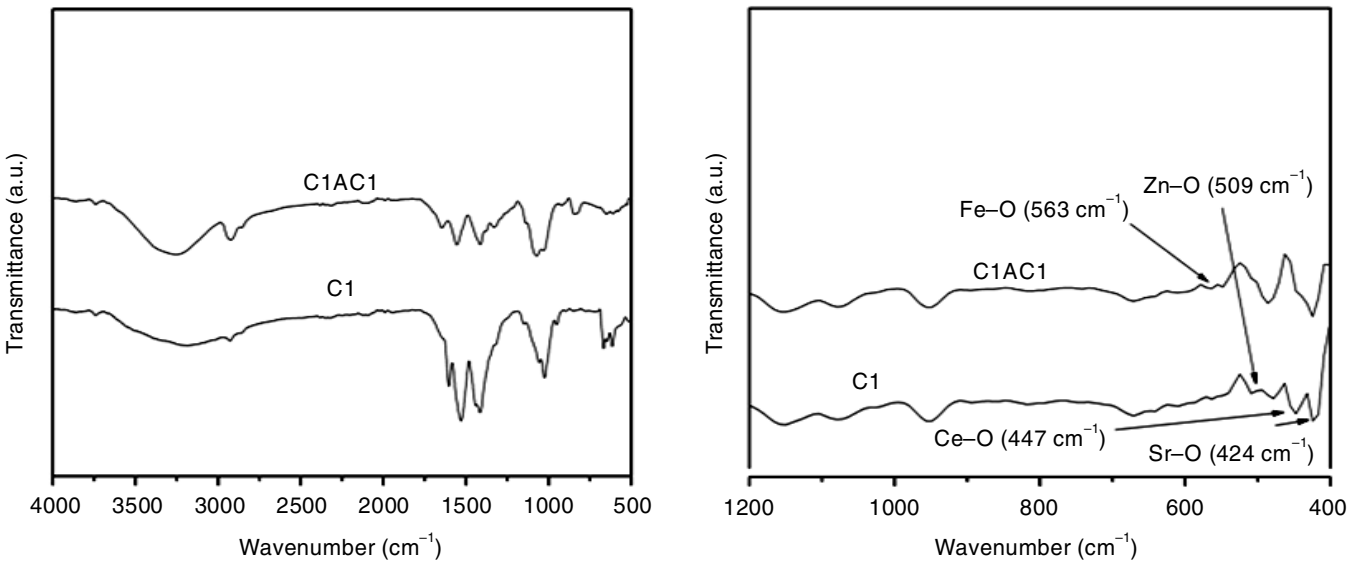

Fig. 1. FT-IR spectra of C1 and C1AC1 thin films

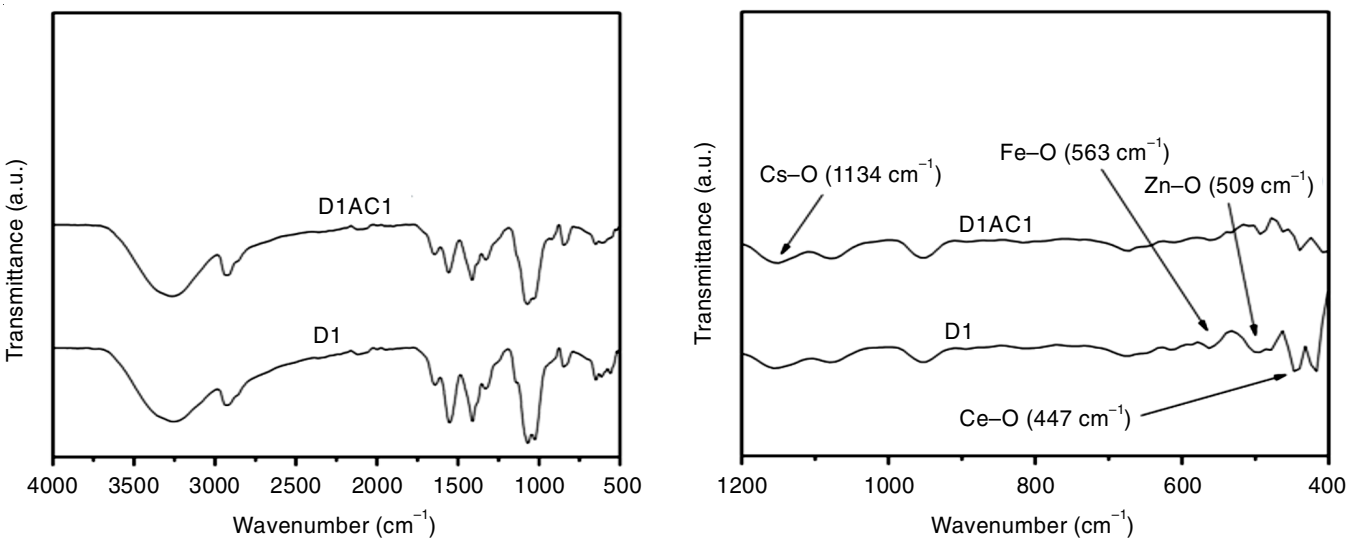

Fig. 2. FT-IR spectra of D1 and D1AC1 thin films

Thermal analysis: The TGA method is used to determine the thermal behaviour of the produced film. Fig. 3 shows the thermal breakdown behaviour of produced films C1, C1AC1 and D1, D1AC1. The whole polymer film undergoes multi-stage thermal decomposition. The first decomposition occurs between 80 and 220 ºC, with a 26% weight loss, which could be attributed to moisture loss. The second decomposition occurs between 220-520 ºC, which could correspond to side chain decay on heating and the third decomposition begins at 520 ºC and ends at 900 ºC, which confirms the loss of the polymer network.

The produced polymer films C1AC1 and D1AC1 contain MONC and DCHP chalcones. Fig. 3 clearly illustrated the breakdown of the added chalcone moiety, which occurs at about 300 ºC. Thermal curves of DCHP added film and other films show a significant difference. Although the thermal breakdown behaviour of the polymer composite film does not differ significantly between C1 and D1 polymer films and metal oxides Sr-O and Cs-O, respectively. Table-2 shows the decomposition percentage as well as three decomposition temperatures. Since, metal oxide nanocomposites are present in all four prepared polymer films, complete decomposition is not observed [27,28].

XRD studies: Figs. 4 and 5 shows the XRD spectra of C1, C1AC1 and D1, D1AC1, with a significant peaks at 2θ of around 20º and 40º, respectively (Table-2). The semi-crystalline character of the prepared thin polymer composite film is reflected. This type of semi-crystalline behaviour for these kinds of films are matched with the literature [26,29,30]. This sort of diffraction pattern was found throughout the whole prepared thin film. Addition of metal oxide to polymers for composite production increases the crystallinity of the polymer [26]. Thus, the addition of doping agents MONC4, MONC5 and DCHP improves the crystallinity of PVA.

SEM studies: Figs. 6 and 7 show SEM images of C1, C1AC1 and D1, D1AC1. The images show smooth surfaces with MONC4, MONC5 and DCHP uniformly dispersed over the surface of polymer matrix. At 5 µm, a bud-like structure was discovered on the surface of thin composite film, while a blossoming flower-like structure was discovered at 1 µm. This type of surface morphological behaviour has already been observed [26,31].

EDX studies: Figs. 8 and 9 show the EDX spectrum of a prepared doped thin polymer film, which reveals the presence of several components in the film. The entire produced film comprises carbon, hydrogen, oxygen, nitrogen and CS polymer impurity (Ca). In addition to the aforementioned elements, the C1 film contains doped metals Fe, Sr, Zn and Ce. The D1 film indicates the presence of doping metals Fe, Cs, Zn and Ce, as well as the previously stated common element. The prepared polymer composite thin film C1AC1, D1AC1 demonstrates the above-mentioned doping metals of C1, D1 and chlorine of doping chalcone. The existence of PVA, CS polymer and MONC4, MONC5 and DCHP chalcone elements is confirmed by EDX analysis.

XPS studies: The presence of various elements with different oxidation states is shown by the XPS of the produced

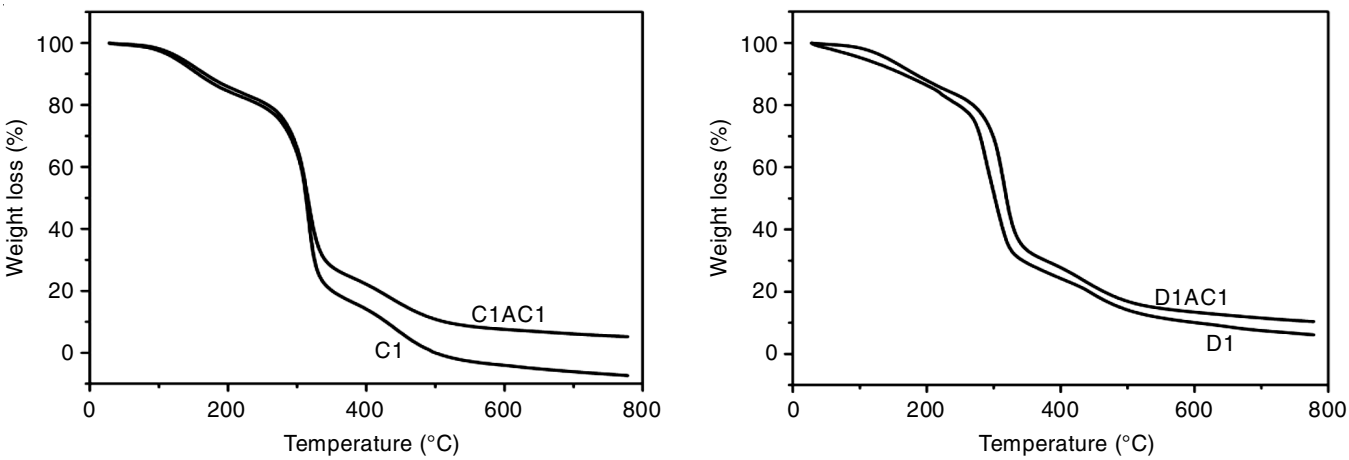

Fig. 3. Thermogram of C1, C1AC1 D1 and D1AC1 thin films

TABLE-2
FT-IR, TGA AND XRD VALUES OF C1, C1AC1, D1 AND D1AC1 THIN FILMS

Analysis		Synthesized thin polymer film			
		C1	C1AC1	D1	D1AC1
FT-IR (cm^{-1})		3177 (OH), 1600 (CO), 1413 (COC), 557 (NH), 563 (Fe-O), 447 (Ce-O), 424 (Sr-O), 509 (Zn-O)	3255 (OH), 1647 (CO), 1552 (CH=CH), 563 (Fe-O), 447 (Ce-O), 424 (Sr-O), 509 (Zn-O	3257(OH), 1647(CO), 1326(COC), 557 (NH), 563 (Fe-O), 447 (Ce-O), 1134(Cs-O), 509 (Zn-O)	3257 (OH), 1647 (CO), 1559 (CH=CH), 563 (Fe-O), 447 (Ce-O), 1134 (Cs-O), 509 (Zn-O)
TGA	1st decomposition (°C)	80-220	80-230	80-200	80-220
	2nd decomposition (°C)	220-520	230-505	200-550	220-520
	3rd decomposition (°C)	520-900	505-900	550-900	520-900
XRD, 2θ		19.6, 40.5	19.5, 40.5	19.7, 41.3	20.5, 40.5

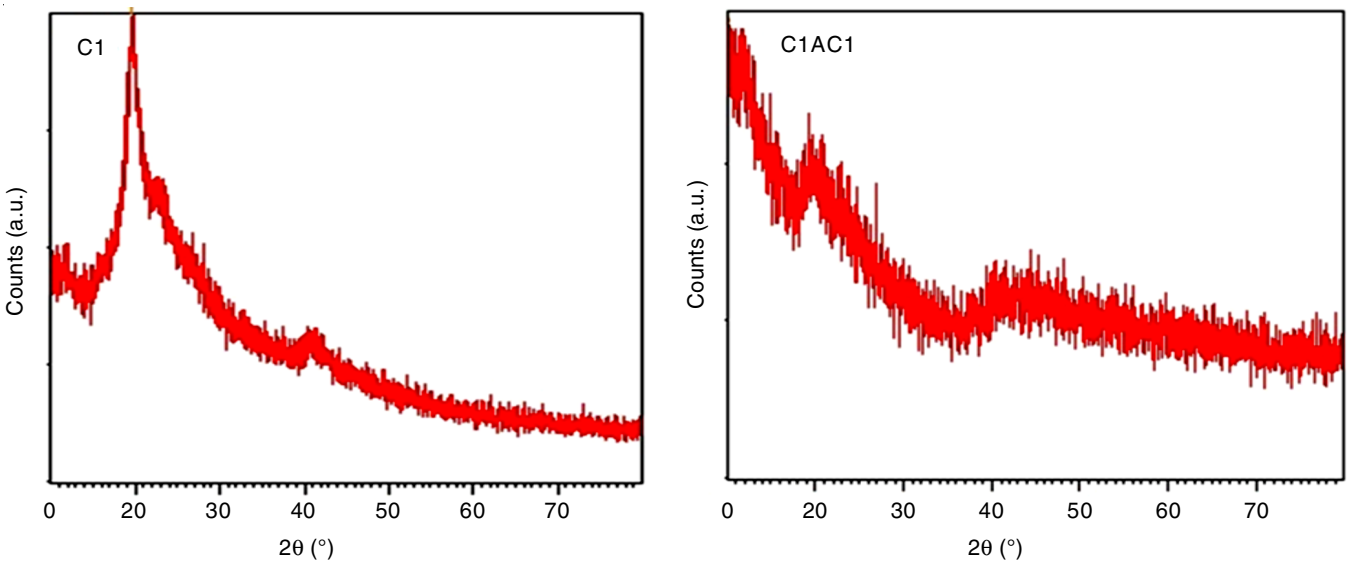

Fig. 4. XRD spectra of C1 and C1AC1 thin films

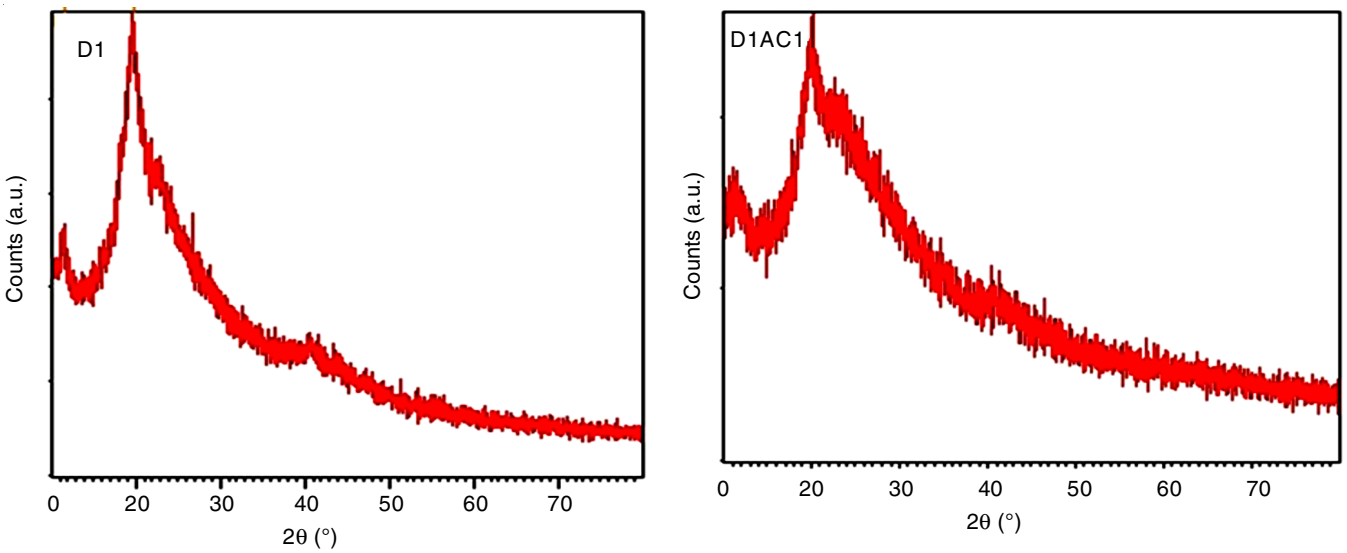

Fig. 5. XRD spectra of D1 and D1AC1 thin films

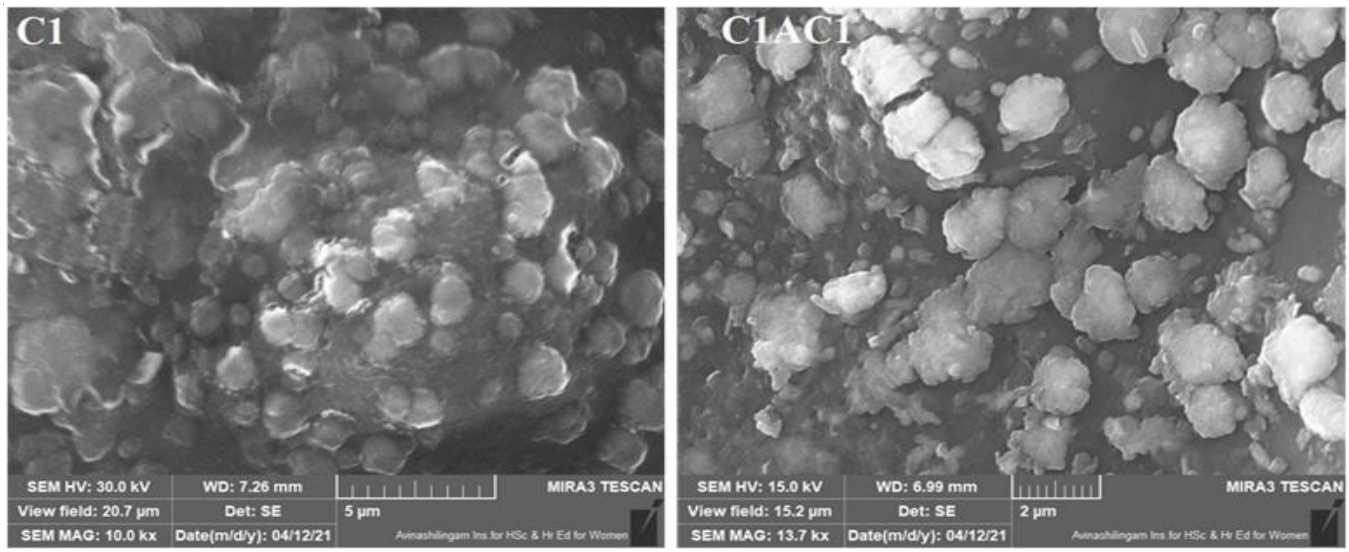

Fig. 6. SEM images of C1 and C1AC1 thin films

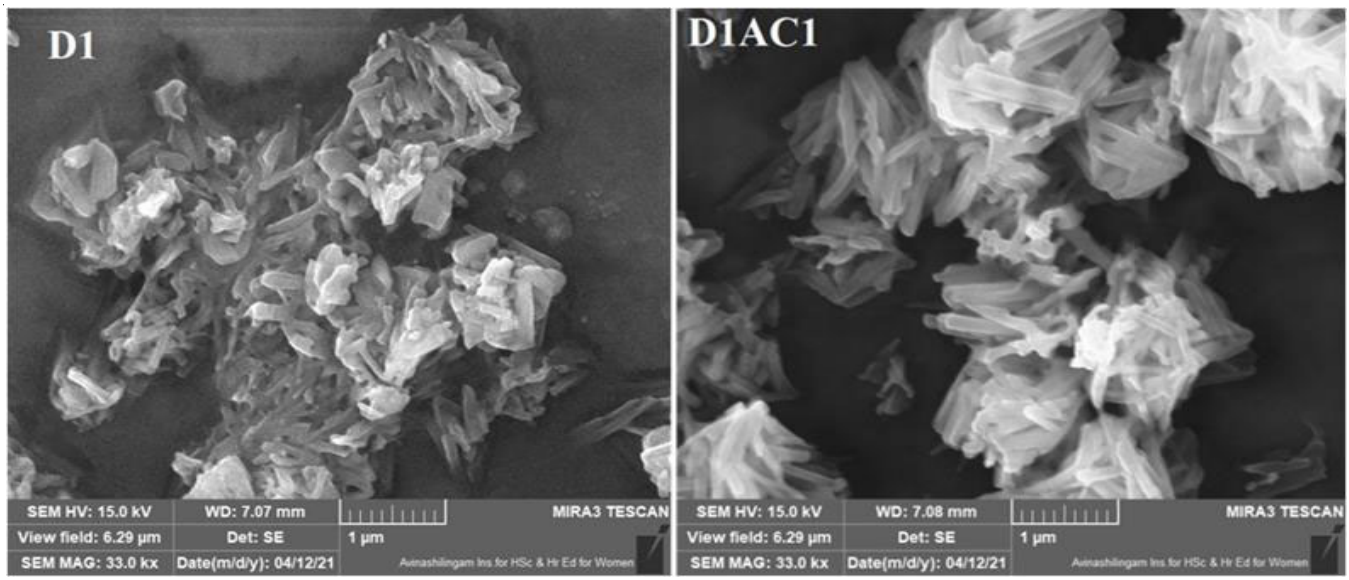

Fig. 7. SEM images of D1 and D1AC1 thin films

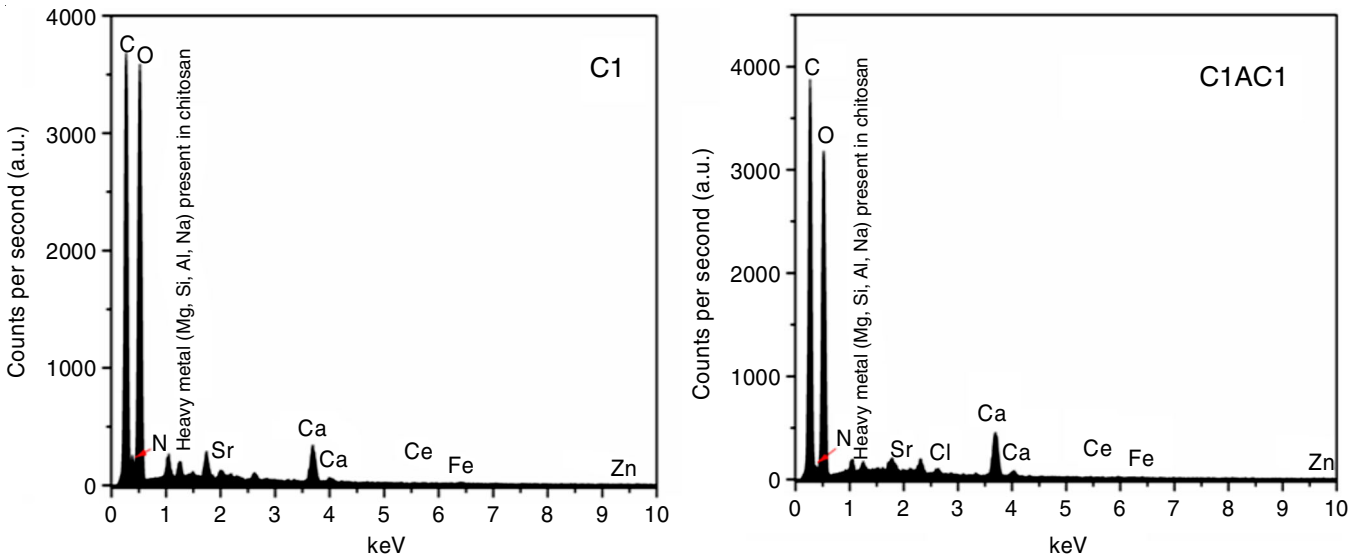

Fig. 8. EDX spectra of C1 and C1AC1 thin films

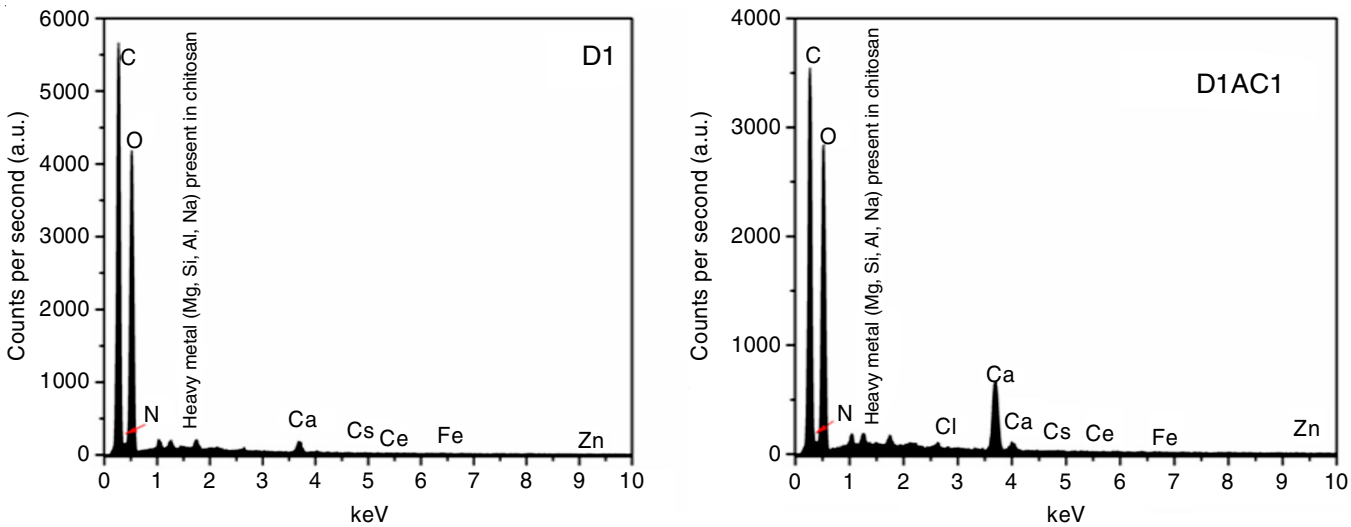

Fig. 9. EDX spectra of D1 and D1AC1 thin films

doped thin polymer films C1 and D1 (Figs. 10 and 11). Figs. 10a and 11a show the survey spectra of MONC4 and MONC5, confirming that the dopant metals are not in the same oxidation state. MONC4 contains the transition metals Ce, Fe, Zn and Sr (Fig. 10). The presence of Ce at binding energy (BEs) of 900.66 eV ($3d_{3/2}$) and 882.13 eV ($3d_{5/2}$) (Fig. 10b) shows its presence within the thin film. The element iron occurs in its +3 oxidation state, which is seen in the XPS spectrum at 718.81 eV ($2p_{1/2}$) and 710.53 eV ($2p_{3/2}$) (Fig. 10c). Sr, on the other hand, emerged in its +2 oxidation state and exhibits two peaks in the XPS

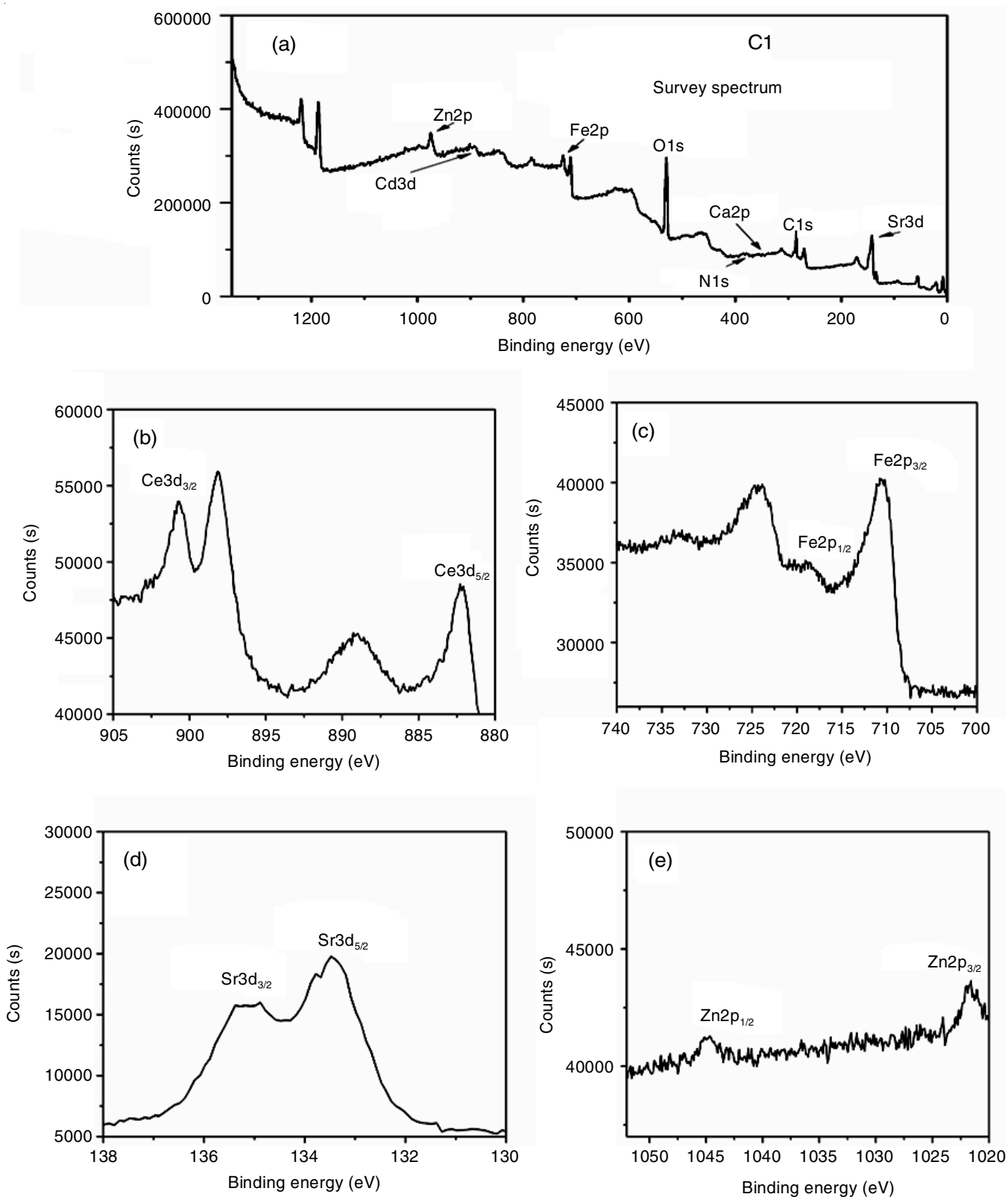

Fig. 10. XPS spectra of C1 (a: survey, b: cerium, c: iron, d: strontium, e: zinc) thin film

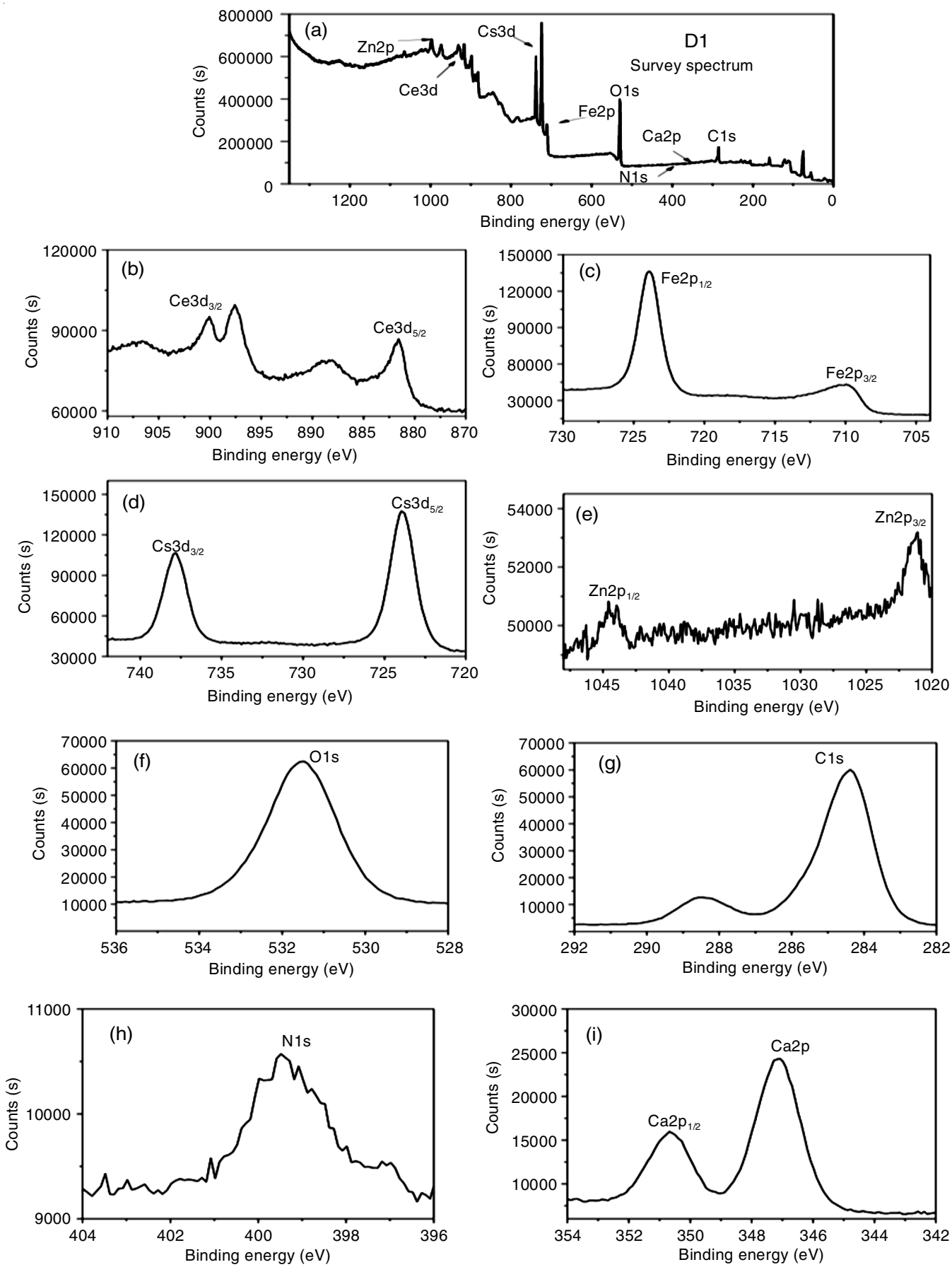

Fig. 11. XPS spectra of D1 (a: survey, b: cerium, c: iron, d: cesium, e: zinc, f: XPS oxygen, g: carbon, h: nitrogen, i: calcium) thin film

spectra, the first at 135.37 eV ($3d_{3/2}$) and the second at 133.49 eV ($3d_{5/2}$) (Fig. 10d). Fig. 10e depicts a zinc XPS spectrum with two distinct peaks, one at 1044.81eV ($2p_{1/2}$) and the other at 1021.61eV ($2p_{3/2}$). These two peaks confirmed that the Zn present in the thin film is in Zn^{2+} oxidation state. The Cs XPS spectra in Fig. 11d shows two prominent peaks, one at 737.73 eV ($3d_{3/2}$) and the other at 724.01 eV ($3d_{5/2}$).

These peaks demonstrate that Cs exists in its +2 oxidation state. Fig. 11f-g show the oxygen and carbon XPS spectra, respectively. Carbon emerged with a BE of 284.45 eV while oxygen appeared at BE of 531.49 eV. The CS nitrogen occurred at 399.41 eV (Fig. 11h), while the CS impurity calcium appeared at 347.13 eV ($2p_{3/2}$) and 350.67 eV ($2p_{1/2}$) (Fig. 11i) [24,26].

Electrical impedance studies: Figs. 12 and 13, depict the produced cole–cole plot of PVA-CS and its doped polymer thin films. At ambient temperature, four prepared thin film impedance graphs display a semi-circle, but at higher temperatures, the semi-circle vanishes, proved that no resistance exist [24]. In the prohibited energy gap, the doping metal ions generate extra energy levels. When the temperature rises, the doped transition metal ions in the polymer matrix become easily excited, resulting in an increase in the number of free electrons. As a result, conductivity increases at higher temperatures as doping enhances the electrical conductivity.

Conduction studies: The conduction spectra are shown in Figs. 14 & 15, which provides the conduction values of the prepared doped thin polymeric composite films C1AC1, D1AC1. Two regions were observed *viz.* (i) a dispersive area at low frequency and (ii) a plateau region at high frequency. As a result, it is evident that the conduction of doped thin polymer film is frequency dependent or the frequency component has a signi-ficant impact on conduction. The conductivity of the prepared polymer composite thin film varies with frequency, although conduction does not alter much at extremely high frequencies, even at greater temperatures, as demonstrated by previous researchers [32] and this type of system obeys the following power law:

$$\sigma_{ac}(\omega) = \sigma_{dc} + A(\omega)^2 \rightarrow 2$$

where dc, A and s denote direct current conductivity, pre-exponential factor (frequency independent), angular frequency and frequency exponent, respectively. The hopping conduction channel is used for film conduction and conductivity varies with temperature, type of historical polymer, doped materials

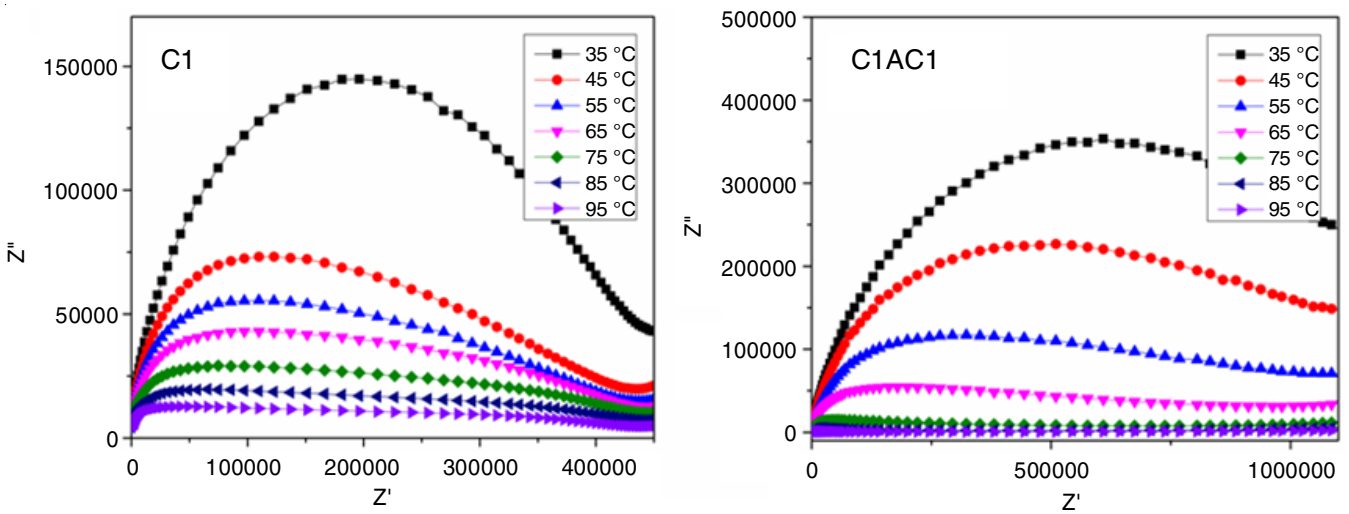

Fig. 12. Cole-Cole spectra of C1 and C1AC1 thin films

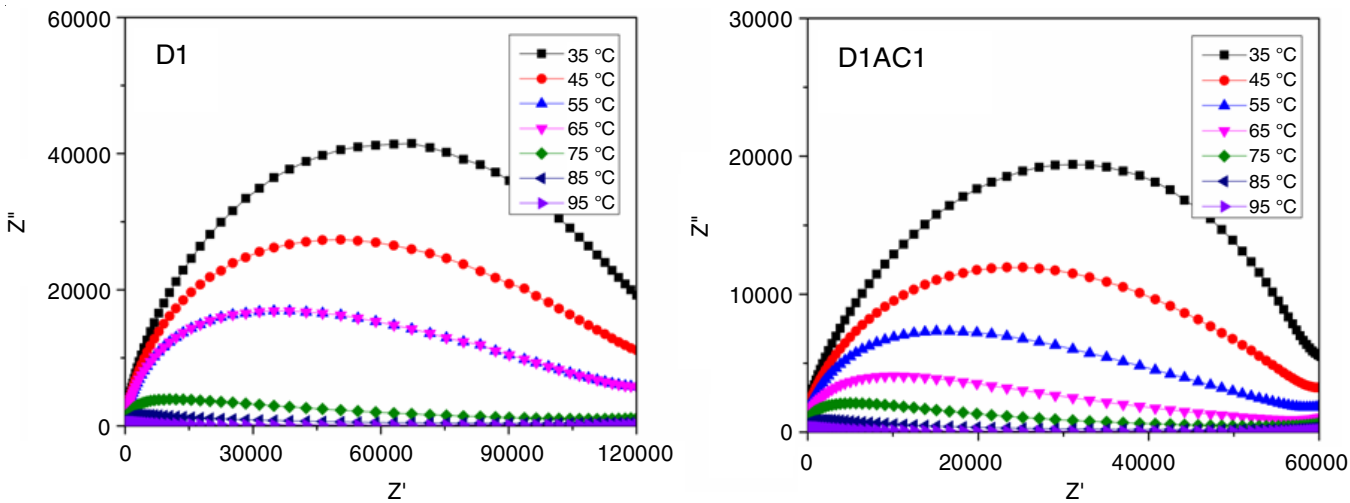

Fig. 13. Cole-Cole spectra of D1 and D1AC1 thin films

and applied frequency [26,32]. Conduction is followed by this type of doped thin polymer film. At the lowest frequency, the measured polymer film has low conductivity. This is due to ion accretion at the interface, which prevents the ions from moving freely, causing conductance to be dispersed. However, increased conduction at high temperatures is caused by the formation of an empty volume in the polymer chain, which allows the ions to flow freely in the host polymer matrix. The C1 film's AC conductance value at room temperature is 2.64×10^{-7}, which is higher than C1AC1's AC conductance value (2.58×10^{-8}) and D1AC1's conductance (3.29×10^{-7}) is also less than D1 (1.12×10^{-6}), indicating that the DCHP chalcone disturbs the conductivity of MONC doped polymer composite film. These results conclude that the presence of organic molecules alone shows very high AC conductance, whereas when mixed with MONC, conductivity decreases (Table-3).

Dielectric studies: The dielectric spectra of a prepared doped thin polymer film clearly demonstrated this frequency-dependent dielectric nature (Figs. 16-19). Tables 4 and 5 show the dielectric values of C1, C1AC1, D1, D1AC1 determined in the low frequency region due to high resistivity and improved interfacial polarization. DCHP chalcone doped with MONC polymer film shows a lesser dielectric value than DCHP undoped polymer film. The doped organic molecules may improve ionic transitions in the polymer matrix. The host PVA also contributes to the improvement of the dielectric properties [26].

TABLE-3
AC CONDUCTIVITY VALUES OF
C1, C1AC1, D1 AND D1AC1 THIN FILMS

Temp. (°C)	AC conductivity (S cm^{-1})			
	C1	C1AC1	D1	D1AC1
35	2.64×10^{-7}	2.58×10^{-8}	1.12×10^{-6}	3.29×10^{-7}
45	5.33×10^{-7}	4.15×10^{-8}	1.83×10^{-6}	4.99×10^{-7}
55	6.66×10^{-7}	7.80×10^{-8}	3.08×10^{-6}	8.34×10^{-7}
65	1.26×10^{-6}	1.71×10^{-7}	1.04×10^{-5}	1.63×10^{-6}
75	1.94×10^{-6}	6.29×10^{-7}	1.11×10^{-5}	3.71×10^{-6}
85	2.86×10^{-6}	3.99×10^{-6}	2.60×10^{-5}	9.23×10^{-6}
95	6.16×10^{-6}	7.05×10^{-6}	6.13×10^{-5}	9.51×10^{-6}

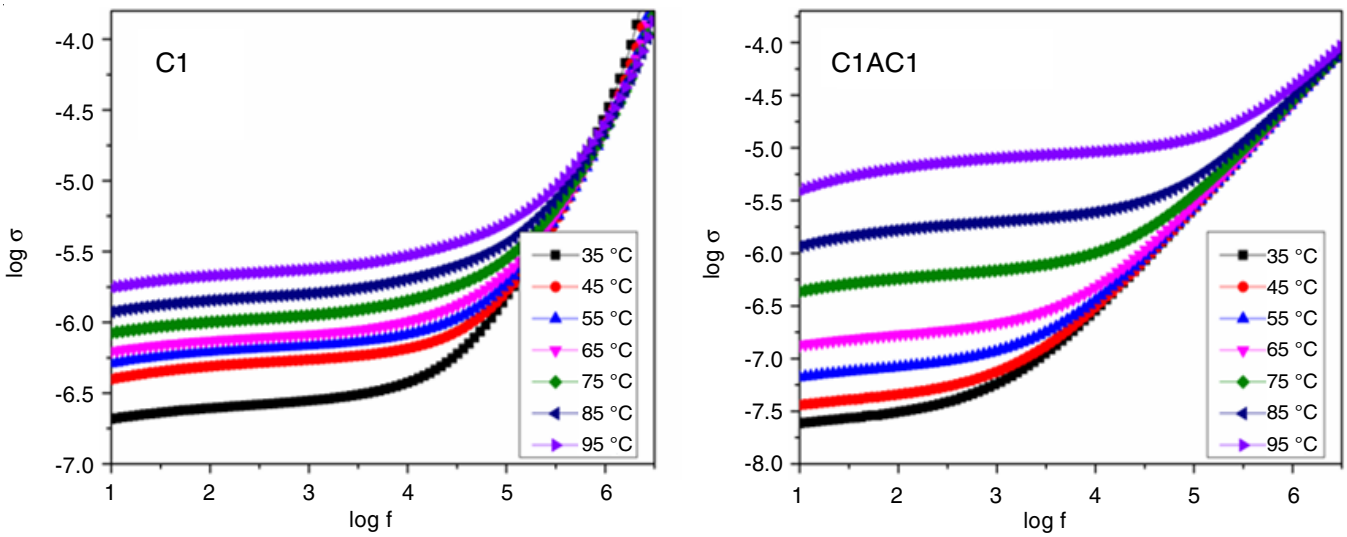

Fig. 14. Conduction spectra of C1 and C1AC1 thin films

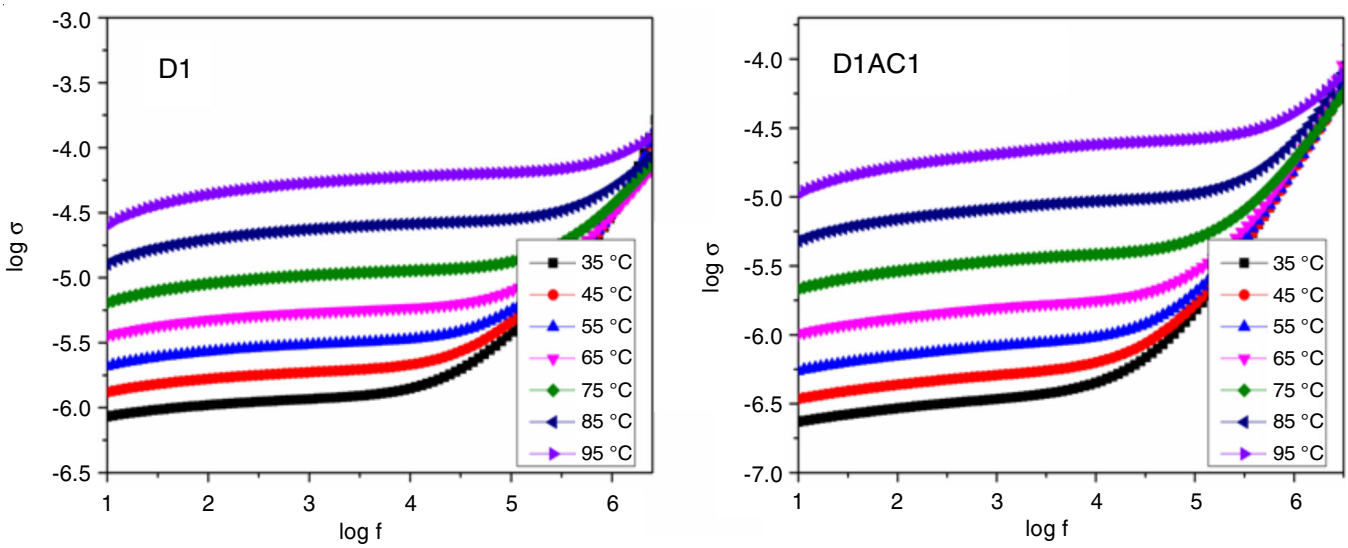

Fig. 15. Conduction spectra of D1 and D1AC1 thin films

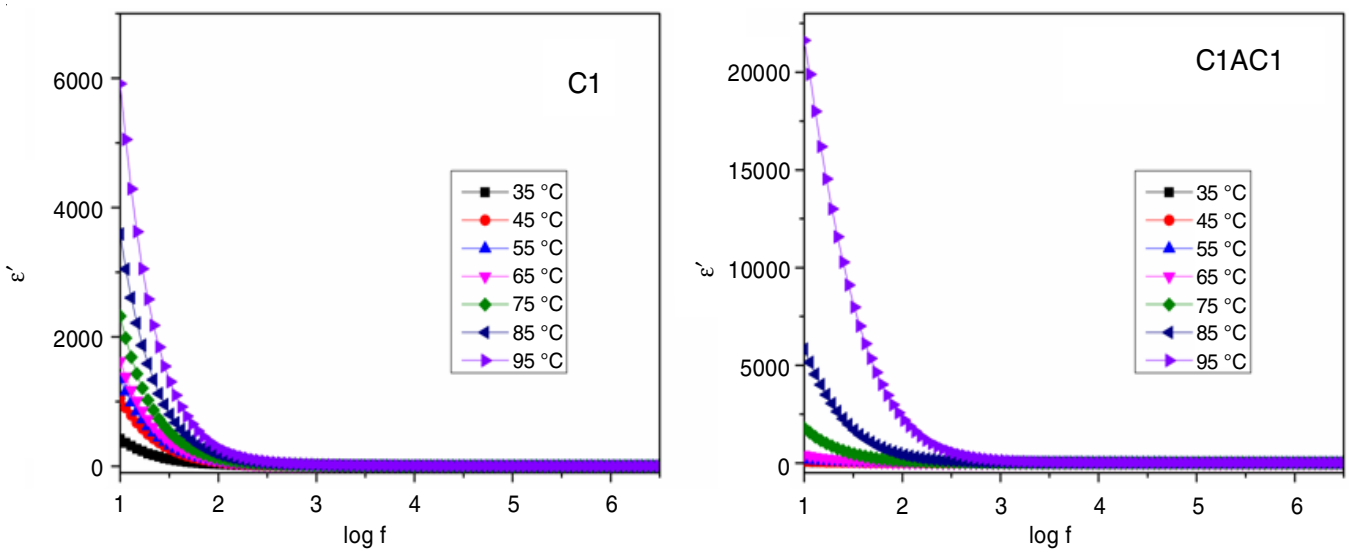

Fig. 16. Dielectric constant spectra of C1 and C1AC1 thin films

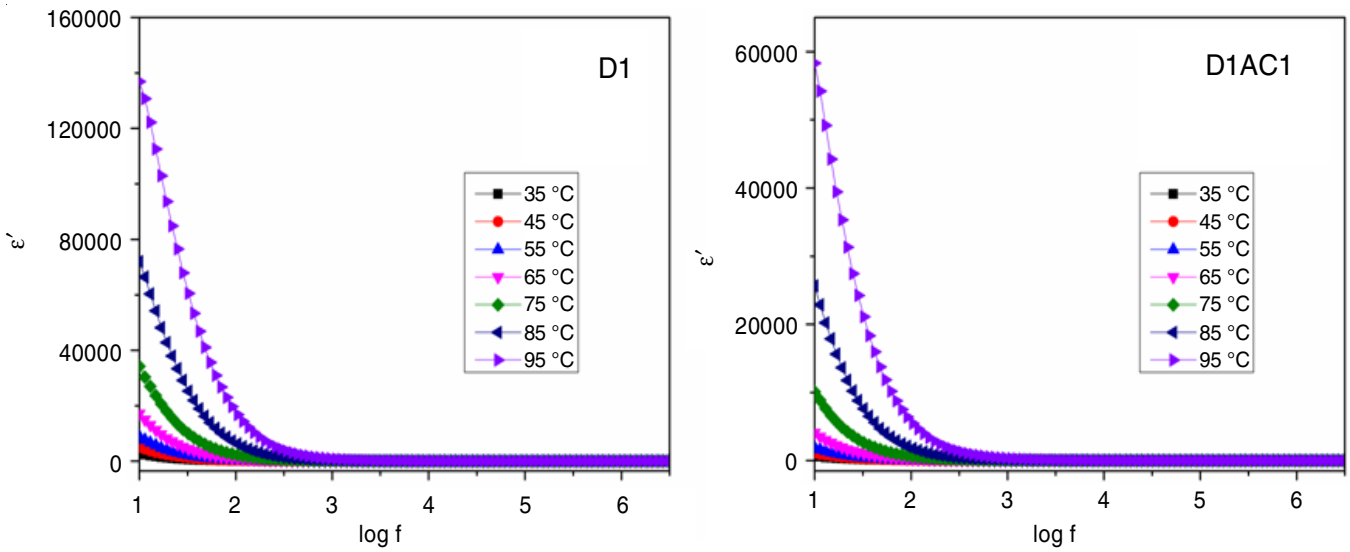

Fig. 17. Dielectric constant spectra of D1 and D1AC1 thin films

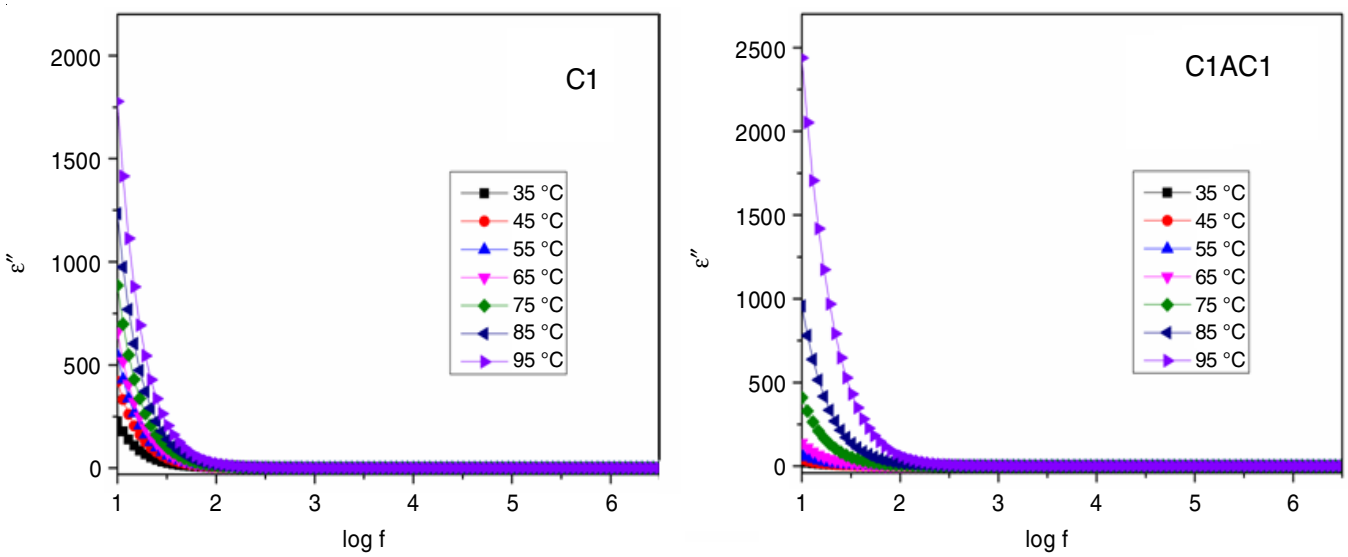

Fig. 18. Dielectric loss spectra of C1 and C1AC1 thin films

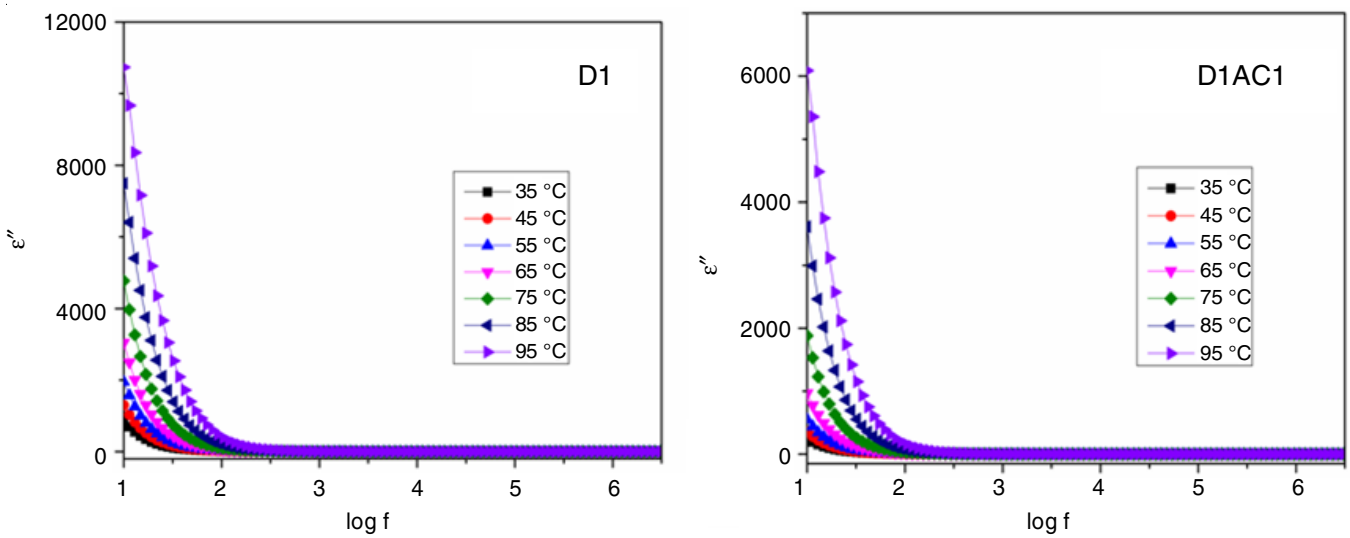

Fig. 19. Dielectric loss spectra of D1 and D1AC1 thin films

TABLE-4
DIELECTRIC CONSTANT VALUES OF
C1, C1AC1, D1 AND D1AC1 THIN FILMS

Temp. (°C)	Dielectric constant			
	C1	C1AC1	D1	D1AC1
35	$4.23 \times 10^{+2}$	$5.41 \times 10^{+1}$	$2.78 \times 10^{+3}$	$6.58 \times 10^{+2}$
45	$1.05 \times 10^{+3}$	$8.51 \times 10^{+1}$	$4.95 \times 10^{+3}$	$1.08 \times 10^{+3}$
55	$1.35 \times 10^{+3}$	$1.75 \times 10^{+2}$	$8.92 \times 10^{+3}$	$1.92 \times 10^{+3}$
65	$1.63 \times 10^{+3}$	$4.13 \times 10^{+2}$	$1.71 \times 10^{+4}$	$4.08 \times 10^{+3}$
75	$2.32 \times 10^{+3}$	$1.79 \times 10^{+3}$	$3.42 \times 10^{+4}$	$1.01 \times 10^{+4}$
85	$5.83 \times 10^{+3}$	$3.59 \times 10^{+3}$	$7.20 \times 10^{+4}$	$2.57 \times 10^{+4}$
95	$2.16 \times 10^{+4}$	$5.92 \times 10^{+3}$	$1.37 \times 10^{+5}$	$5.83 \times 10^{+4}$

TABLE-5
DIELECTRIC LOSS VALUES OF
C1, C1AC1, D1 AND D1AC1 THIN FILMS

Temp. (°C)	Dielectric loss			
	C1	C1AC1	D1	D1AC1
35	$2.26 \times 10^{+2}$	$2.62 \times 10^{+1}$	$8.74 \times 10^{+2}$	$2.46 \times 10^{+2}$
45	$4.20 \times 10^{+2}$	$3.89 \times 10^{+1}$	$1.30 \times 10^{+3}$	$3.53 \times 10^{+2}$
55	$5.46 \times 10^{+2}$	$7.07 \times 10^{+1}$	$1.95 \times 10^{+3}$	$5.50 \times 10^{+2}$
65	$6.60 \times 10^{+2}$	$1.39 \times 10^{+2}$	$3.05 \times 10^{+3}$	$9.69 \times 10^{+2}$
75	$8.85 \times 10^{+2}$	$4.10 \times 10^{+2}$	$4.78 \times 10^{+3}$	$1.88 \times 10^{+3}$
85	$1.23 \times 10^{+3}$	$9.57 \times 10^{+2}$	$7.49 \times 10^{+3}$	$3.61 \times 10^{+3}$
95	$3.78 \times 10^{+3}$	$2.44 \times 10^{+3}$	$1.07 \times 10^{+4}$	$6.09 \times 10^{+3}$

Conclusion

To prepare conducting thin polymeric composite films, polyvinyl alcohol (PVA), chitosan (CS) and doping agents DCHP, MONC4 and MONC5 were used. The characteristics of four prepared films were characterized using FT-IR, TGA, XRD, EDX, XPS and SEM analysis. Studies showed that there was no chemical interaction between the host polymer and the doping compounds MONC4 and MONC5 or DCHP. Due to the good thermal stability, the polymeric composite films experienced multi-stage decomposition when heated. The doping agents were dispersed uniformly throughout the polymeric matrix. The SEM pictures of the films revealed a blooming-bud-like structure, whereas XRD examination verifies the polymer matrix's semi-crystalline structure, while EDX and XPS analyses show the presence of the different elements present in the film. The XPS analysis also revealed information about the oxidation state of the added metals. At ambient temperature, the prepared polymer film having both metal oxide nanocomposite and chalcone revealed an excellent AC conductance (1.12×10^{-6} S cm^{-1}).

CONFLICT OF INTEREST

The authors declare that there is no conflict of interests regarding the publication of this article.

REFERENCES

1. N. Burger, A. Laachachi, M. Ferriol, M. Lutz, V. Toniazzo and D. Ruch, *Prog. Polym. Sci.*, **61**, 1 (2016); https://doi.org/10.1016/j.progpolymsci.2016.05.001
2. H. Pang, L. Xu, D.X. Yan and Z.M. Li, *Prog. Polym. Sci.*, **39**, 1908 (2014); https://doi.org/10.1016/j.progpolymsci.2014.07.007
3. H. Deng, L. Lin, M. Ji, S. Zhang, M. Yang and Q. Fu, *Prog. Polym. Sci.*, **39**, 627 (2014); https://doi.org/10.1016/j.progpolymsci.2013.07.007
4. X. Liu, C. Li, Y. Pan, D.W. Schubert and C. Liu, *Composites B Eng.*, **164**, 37 (2019); https://doi.org/10.1016/j.compositesb.2018.11.054
5. X. Liu, Y. Pan, G. Zheng and D.W. Schubert, *Sci. Technol.*, **128**, 1 (2016); https://doi.org/10.1016/j.compscitech.2016.03.011
6. Y. Li, B. Zhou, G. Zheng, X. Liu, T. Li, C. Yan, C. Cheng, K. Dai, C. Liu, C. Shen and Z. Guo, *J. Mater. Chem. C Mater. Opt. Electron. Devices*, **6**, 2258 (2018); https://doi.org/10.1039/C7TC04959E
7. L. Sha, Z. Chen, Z. Chen, A. Zhang and Z. Yang, *Int. J. Polym. Sci.*, **2016**, 1 (2016); https://doi.org/10.1155/2016/6869154
8. Z. Azwa, B. Yousif, A. Manalo and W. Karunasena, *Mater. Des.*, **47**, 424 (2013); https://doi.org/10.1016/j.matdes.2012.11.025
9. J.K. Pandey and R.P. Singh, *Stärke*, **57**, 8 (2005); https://doi.org/10.1002/star.200400313
10. K. Deshmukh, M.B. Ahamed, R.R. Deshmukh, S.K. Khadheer Pasha, P.R. Bhagat and K. Chidambaram, *Biopolym. Compos. Electr.*, **3**, 27 (2017); https://doi.org/10.1016/B978-0-12-809261-3.00003-6

11. H.M. Shiri and A. Ehsani, *Bull. Chem. Soc. Jpn.*, **89**, 1201 (2016); https://doi.org/10.1246/bcsj.20160082
12. C.-T. Huang, L. Kumar Shrestha, K. Ariga and S. Hsu, *J. Mater. Chem. B Mater. Biol. Med.*, **5**, 8854 (2017); https://doi.org/10.1039/C7TB01594A
13. M. Dai Prè, A. Martucci, D.J. Martin, S. Lavina and V. Di Noto, *J. Mater. Sci.*, **50**, 2218 (2015); https://doi.org/10.1007/s10853-014-8784-0
14. S. Kumar, B. Krishnakumar, A. Sobral and J. Koh, *Carbohydr. Polym.*, **205**, 559 (2019); https://doi.org/10.1016/j.carbpol.2018.10.108
15. A.I.Y. Tok, L.H. Luo, F.Y.C. Boey and J.L. Woodhead, *J. Mater. Res.*, **21**, 119 (2006); https://doi.org/10.1557/jmr.2006.0024
16. A. Martínez Arias, A.B. Hungría, M. Fernández García, J.C. Conesa and G. Munuera, *J. Phys. Chem. B*, **108**, 17983 (2004); https://doi.org/10.1021/jp0465837
17. D. Barreca, A. Gasparotto, C. Maccato, C. Maragno, E. Tondello, E. Comini and G. Sberveglieri, *Nanotechnology*, **18**, 125502 (2007); https://doi.org/10.1088/0957-4484/18/12/125502
18. K. Sohlberg, S.T. Pantelides and S.J. Pennycook, *J. Am. Chem. Soc.*, **123**, 6609 (2001); https://doi.org/10.1021/ja004008k
19. C.C. Hsieh, A. Roy, A. Rai, Y.F. Chang and S.K. Banerjee, *Appl. Phys. Lett.*, **106**, 173108 (2015); https://doi.org/10.1063/1.4919442
20. E.K. Hollmann, S.V. Razumov and A.V. Tumarkin, *Tech. Phys. Lett.*, **25**, 440 (1999); https://doi.org/10.1134/1.1262509
21. A. Corma, P. Atienzar, H. García and J.Y. Chane-Ching, *Nat. Mater.*, **3**, 394 (2004); https://doi.org/10.1038/nmat1129
22. R. Ravindranath, P.K. Ajikumar, N.B. Muhammad Hanafiah, W. Knoll and S. Valiyaveettil, *Chem. Mater.*, **18**, 1213 (2006); https://doi.org/10.1021/cm052121+
23. E. Arias Marin, J. Le Moigne, T. Maillou, D. Guillon, I. Moggio and B. Geffroy, *Macromolecules*, **36**, 3570 (2003); https://doi.org/10.1021/ma020121e
24. V. Thangaraj, M. Yogapriya, K. Thirumalai, S. Suresh, M. Swaminathan, A. Sundaramurthy, R. Nandhakumar, E. Vakees and A. Araichimani, *ACS Omega*, **3**, 16509 (2018); https://doi.org/10.1021/acsomega.8b02817
25. J. Suresh, E. Vakees, S. Karthik, M. Kayalvizhi and A. Arun, *Designed Monomers*, **17**, 753 (2014); https://doi.org/10.1080/15685551.2014.918014
26. S. Karthik, J. Suresh, P. Saravanan and A. Arun, *J. Sci. Adv. Mater. Devices*, **5**, 400 (2020); https://doi.org/10.1016/j.jsamd.2020.05.006
27. F.S. Kittur, K.V.H. Prashanth, K.U. Sankar and R.N. Tharanathan, *Carbohydr. Polym.*, **49**, 185 (2002); https://doi.org/10.1016/S0144-8617(01)00320-4
28. A.G. Yavuz, A. Uygun and H.K. Can, *Carbohydr. Res.*, **346**, 2063 (2011); https://doi.org/10.1016/j.carres.2011.06.009
29. S.B. Aziz, *J. Electron. Mater.*, **45**, 736 (2016); https://doi.org/10.1007/s11664-015-4191-9
30. S. Kumar, P.K. Dutta and J. Koh, *Int. J. Biol. Macromol.*, **49**, 356 (2011); https://doi.org/10.1016/j.ijbiomac.2011.05.017
31. T.C.S. Shetty, S. Raghavendra and S.M. Dharmaprakash, *Mater. Today Proc.*, **3**, 2163 (2016); https://doi.org/10.1016/j.matpr.2016.04.122
32. S. Karthik, J. Suresh, S. Selvasekarapandian, S. Shanmugasundaram, V. Thangaraj, K. Balaji and A. Arun, *Appl. Sci.*, **1**, 1371 (2019); https://doi.org/10.1007/s42452-019-1432-1